





Cite this: *Phys. Chem. Chem. Phys.*,  
2022, 24, 21188

# Analysis of the ignition of hydrogen/air mixtures induced by a hot particle

Yan Wang,<sup>a</sup> Shangpeng Li,<sup>b</sup> Yiqing Wang, <sup>a</sup> Dehai Yu, <sup>\*a</sup> Huangwei Zhang<sup>b</sup> and Zheng Chen<sup>a</sup>

Understanding the ignition and explosion of hydrogen induced by a hot particle is crucial for the safety of hydrogen storage, transmission and utilization. In this paper, the ignition/explosion of hydrogen/air mixtures induced by a hot particle is investigated theoretically and numerically. Eigenvalue analysis is conducted for the radical-runaway ignition process in which a detailed reaction mechanism is considered. The governing equation for radical accumulation is converted into a rate-controlling ordinary differential equation (ODE). The ODE can be solved with the help of a hypothetical single-step reaction model, whose kinetic characteristics are related to the positive eigenvalue of the rate matrix constituted by relevant linear chain reactions. Based on the single-step reaction model, the critical ignition Damköhler number can be determined. Besides, transient simulations are conducted using in-house code A-SURF, in which detailed chemistry and transport are considered. The critical ignition temperatures predicted by eigenvalue analysis agree well with experimental data reported in the literature and present numerical results over a wide range of particle radii. The particle surface introduces temperature inhomogeneity in the ignition of a hydrogen/air mixture, which yields a Z-shaped curve of the explosion limit. The Z-shaped curve shifts to a higher temperature and pressure regime along the boundary of the second explosion limit when the particle size decreases. The increasing difficulty in the ignition can be attributed to the strengthening of radical diffusion as the particle becomes smaller. Compared to a homogeneous ignition system, the presence of a particle surface can alter the relative impacts among key chain reactions. The effects of preferential diffusion between heat and mass transport (*i.e.*, Lewis number effect) and equivalence ratio on the Z-shaped curve of the explosion limit are assessed and interpreted. The present study provides useful insights into the kinetics and transport involved in the ignition of hydrogen/air mixtures by a hot particle, which is closely related to the fire/explosion safety of hydrogen.

Received 27th May 2022,  
Accepted 9th August 2022

DOI: 10.1039/d2cp02409h

rsc.li/pccp

## 1. Introduction

A hot particle is a potential thermal source leading to ignition in flammable mixtures.<sup>1</sup> Understanding hot particle induced ignition is crucial not only for fundamental combustion research but also for fire safety control.<sup>2,3</sup>

Recently, hydrogen has drawn soaring attention due to zero carbon emission.<sup>4,5</sup> Massive utilization of hydrogen as fuel requires its storage and transportation at a high safety level.<sup>6</sup> Because of the small molecular weight, hydrogen is highly dispersive and has a high risk of leakage from a container. In addition, hydrogen has much lower ignition energy, a wider

range of flammability limit and higher flame speed,<sup>7–9</sup> compared with conventional hydrocarbon fuels. The presence of hot particles could induce accidental ignition and explosion of hydrogen, which leads to severe safety issues for hydrogen storage, transport, and utilization.<sup>6</sup>

Studies on the ignition of hydrogen/air and hydrocarbon/air mixtures by hot particles have been widely conducted. Silver<sup>10</sup> measured the minimum ignition temperature for spherical hot particles injected into a combustible mixture. Roth *et al.*<sup>11,12</sup> investigated the ignition of hydrogen/air mixtures by laser-heated particles with different materials and sizes. Coronel *et al.*<sup>13</sup> conducted a series of both experimental and numerical studies, in which a hot particle falls into a flammable mixture containing hydrogen or *n*-hexane leading to ignition. They found that the ignition process is affected by a thermal boundary layer on the particle surface developed from the flow of the reactant mixture. Recently, simulations considering detailed chemistry and transport have been conducted for

<sup>a</sup> SKLTCS, CAPT, BIC-ESAT, Department of Mechanics and Engineering Science, College of Engineering, Peking University, Beijing 100871, P. R. China.  
E-mail: dehai.yu@pku.edu.cn

<sup>b</sup> Department of Mechanical Engineering, National University of Singapore, Singapore 117576, Singapore

particle-induced ignition of different fuels.<sup>14–17</sup> It is demonstrated that chemical kinetics play important roles in determining the minimum ignition temperature of the hot particle.

Nevertheless, most experimental and numerical studies<sup>10–19</sup> on the ignition of hydrogen by hot particles are restricted to certain conditions *e.g.*, initial temperature, pressure and equivalence ratio. For practical interest, it is attractive to derive an expression that can quantitatively describe the ignition behaviour over a wide range of relevant parameters. So far, such investigation is still not in place, which motivates the present study.

Adopting asymptotic analysis, Law<sup>20</sup> proposed an ignition criterion in terms of a reduced Damköhler number, denoted by  $\Delta_I$ , for hot particle induced ignition in a quiescent combustible mixture. For  $\Delta_I > 1$ , heat release from chemical reactions dominates over the conductive heat loss on the hot surface, and thereby ignition occurs. The critical ignition condition is characterized by  $\Delta_I = 1$ . Since  $\Delta_I$  is determined based on a single-step, overall irreversible reaction, the theoretical model cannot accurately describe the ignition characteristics of hydrogen/air mixtures, which essentially involve multiple radical chain reactions.<sup>7,8</sup> Yu and Chen<sup>21</sup> theoretically investigated particle ignition in a flowing environment, the flow convection enhances the radical loss on the particle surface and suppresses ignition. At conditions of  $Re \ll 1$ , the flow tends to accumulate thermal energy on the rear hemisphere and facilitates ignition at the rear stagnation point. As  $Re$  continuously increases, flow separation originates and moves upstream. With increasing  $Re$  number, the critical ignition temperature becomes higher.

Because of the interactions among radical reactions of hydrogen oxidization,<sup>7</sup> the ignition/explosion limit exhibits Z-shaped curves in the  $p$ – $T$  space. Recently, analytical expressions have been derived for the three ignition limits focusing on the radical-runaway ignition of hydrogen. Wang and Law<sup>22</sup> derived the theoretical expression of the Z-curve for a homogeneous system. Liang and Law<sup>23</sup> improved the reaction mechanisms by incorporating nonlinear reactions. Li *et al.*<sup>24</sup> then successfully extended their theoretical model to inhomogeneous, strained counterflows. The above theoretical studies provide valuable insights into the underlying mechanism leading to the non-monotonic ignition limits of hydrogen.

In this work, the ignition of hydrogen/air mixtures by hot particles is analytically and numerically studied. The formulation describing the ignition process is provided in Section 2. Based on eigenvalue analysis, the analytical solution of the radical equation and the critical ignition condition is derived. Adopting this method, the effects of various parameters, such as radical wall destruction, particle size, equivalence ratio and Lewis number, on the Z-shaped ignition limit and the critical ignition temperature are discussed in Section 3. Numerical simulations considering detailed chemistry and transport properties are conducted to validate the theoretical results. The reaction sensitivity is also investigated to acquire insights into the difference between particle ignition and homogeneous ignition. The conclusion is given in Section 4.

## 2. Formulation

Here we consider a hot particle suspended in a quiescent hydrogen/air mixture, which is similar to Roth *et al.*'s experimental setup.<sup>11,12</sup> The environmental mixture can be ignited by the hot particle with sufficiently high temperatures.

In theoretical analysis, we consider radical-runaway ignition. A detailed reaction mechanism is listed in Table 1. The rate coefficients can be found in ref. 24. Besides, the effective wall destruction of radicals, which can affect the ignition limit,<sup>23</sup> is taken into account.

To validate the theoretical results, we simulate the transient ignition of  $H_2$ /air mixtures by a hot particle using the in-house code A-SURF,<sup>25–27</sup> in which detailed hydrogen chemistry<sup>28</sup> and transport properties are included. The computation domain is 50 cm in length, which ensures the constancy of pressure during the ignition process. An adaptive mesh refinement technique is adopted to resolve the thermal boundary layer near the hot surface and the reaction zone. The finest mesh size is 4  $\mu\text{m}$ , and the corresponding time step is 1 ns. More details on the numerical approach can be found in ref. 17.

### 2.1 Chemically-frozen model in the pre-ignition stage

Prior to ignition, the heat release from the chemical reaction is negligible.<sup>22,23</sup> The temperature and reactant species equations, as well as the boundary conditions are

$$\begin{cases} \frac{1}{r^2} \frac{d}{dr} \left( r^2 \lambda \frac{dT}{dr} \right) = 0, \\ \frac{1}{r^2} \frac{d}{dr} \left( r^2 D \frac{dY_i}{dr} \right) = 0, \\ r = R: T = T_p, Y_F = Y_{F,u}, Y_O = Y_{O,u}, \\ r \rightarrow \infty: T = T_u, Y_F = Y_{F,u}, Y_O = Y_{O,u}, \end{cases} \quad (1)$$

where  $\lambda$  is the thermal conductivity,  $D$  is the mass diffusion

**Table 1** The adopted  $H_2/O_2$  reaction mechanism, with the reaction rate coefficient:  $k(T) = BT^\alpha e^{-T_a/T}$  from ref. 8, 23 and 24

No.	Reaction	$B$ (cm, mol, s, K)	$\alpha$	$T_a$ (K)
Initial reaction				
R6b	$H_2 + O_2 \rightarrow HO_2 + H$	$2.69 \times 10^{12}$	0.36	27 888
Linear chain reactions				
R1f	$H + O_2 \rightarrow O + OH$	$3.52 \times 10^{16}$	−0.7	8590
R2f	$H_2 + O \rightarrow OH + H$	$5.06 \times 10^4$	2.67	3165
R3f	$H_2 + OH \rightarrow H_2O + H$	$1.17 \times 10^9$	1.3	1825
R4f	$H + O_2 + M \rightarrow HO_2 + M$	$k_0$	−1.4	0
		$k_\infty$	0.44	0
		$k_0$	−4.2	25 703
R10f	$H_2O_2 + M \rightarrow 2OH + M$	$k_0$	−1.27	25 703
		$k_\infty$	0.61	12 045
R12f	$HO_2 + H_2 \rightarrow H_2O_2 + H$	$7.80 \times 10^{10}$	0.61	12 045
Nonlinear chain reactions				
R5f	$HO_2 + H \rightarrow 2OH$	$7.08 \times 10^{13}$	0	148
R6f	$HO_2 + H \rightarrow H_2 + O_2$	$1.66 \times 10^{13}$	0	414
R9f	$H + H + M \rightarrow H_2 + M$	$1.30 \times 10^{18}$	−1	0
R11f	$HO_2 + HO_2 \rightarrow H_2O_2 + O_2$	$1.03 \times 10^{14}$	0	5556
		$1.94 \times 10^{11}$	0	−709
R13f	$HO_2 + OH \rightarrow H_2O + O_2$	$2.89 \times 10^{13}$	0	−252
R14f	$H_2O_2 + H \rightarrow H_2O + OH$	$2.41 \times 10^{13}$	0	1998
R15f	$HO_2 + O \rightarrow O_2 + OH$	$3.25 \times 10^{13}$	0	0

coefficient of the reactant mixture,  $T_p$  is the particle temperature,  $T_u$  is the environment temperature,  $Y_i$  is the mass fraction of species  $i$  (F for  $H_2$  and O for  $O_2$ ) and  $R$  is the particle radius. By solving eqn (1) we obtain the chemically-frozen solution (denoted by subscript Fr) as

$$\begin{cases} T_{Fr} = T_p(1 - \beta\zeta) \\ Y_{H_2,Fr} = Y_{H_2,u} \\ Y_{O_2,Fr} = Y_{O_2,u} \end{cases} \quad (2)$$

where  $\beta = (T_p - T_u)/T_p$  is the expansion ratio and  $\zeta = 1 - R/r$  is the normalized distance.

## 2.2 Governing equations of radical accumulation

During the ignition process, the consumption of reactant creates key radicals, *i.e.*, H, O, OH,  $HO_2$  and  $H_2O_2$ , whose relative variations decisively affect the ignition outcome. Since the concentrations of radicals are considerably lower than

under very high-pressure conditions.<sup>24</sup> Neglecting the non-linear chain reactions, the governing equations for radical accumulation are simplified to

$$\frac{d^2 Y}{d\zeta^2} = -\frac{R^2}{\rho D_Y(1 - \zeta)^4} W \{LX + I\}. \quad (3)$$

Here  $Y = (Y_H, Y_O, Y_{OH}, Y_{HO_2}, Y_{H_2O_2})^T$  and  $X = ([H], [O], [OH], [HO_2], [H_2O_2])^T$  are the mass fraction and molar concentration vectors, respectively.  $D_Y$  refers to the molar-averaged diffusion coefficient of radicals and is regarded as constant at a given composition of the mixture. The conversion between the molar and mass fraction vectors is described by  $X = \rho W^{-1}Y$ , where  $W = \text{diag}(W_H, W_O, W_{OH}, W_{HO_2}, W_{H_2O_2})$  is a diagonal matrix consisting of molecular weights of individual radicals. The column vector  $I = (k_{6b}[H_2][O_2], 0, 0, k_{6b}[H_2][O_2], 0)^T$  refers to the initiation reactions involving reactants only. The matrix  $L$  represents the sets of linear chain reactions (reactant–radical) and radical wall destruction reactions (wall–radical), which are listed in the following part.

$$L = \begin{bmatrix} -k_{1f}[O_2] - k_{4f}[O_2][M] - k_H & k_{2f}[H_2] & k_{3f}[H_2] & k_{12f}[H_2] & 0 \\ k_{1f}[O_2] & -k_{2f}[H_2] - k_O & 0 & 0 & 0 \\ k_{1f}[O_2] & k_{2f}[H_2] & -k_{3f}[H_2] - k_{OH} & 0 & 2k_{10f}[M] \\ k_{4f}[O_2] & 0 & 0 & -k_{12f}[H_2] - k_{HO_2} & 0 \\ 0 & 0 & 0 & k_{12f}[H_2] & -k_{10f}[M] - k_{H_2O_2} \end{bmatrix}$$

those of the original reactants before ignition, the nonlinear reactions, involving quadratic terms of radical concentrations, exhibit insubstantial impacts on the ignition process except

The elements of matrix  $L$  are constituted by the reaction rate coefficients and concentrations of reactants and inert gases, denoted by  $M$ . The particle temperature is significantly higher

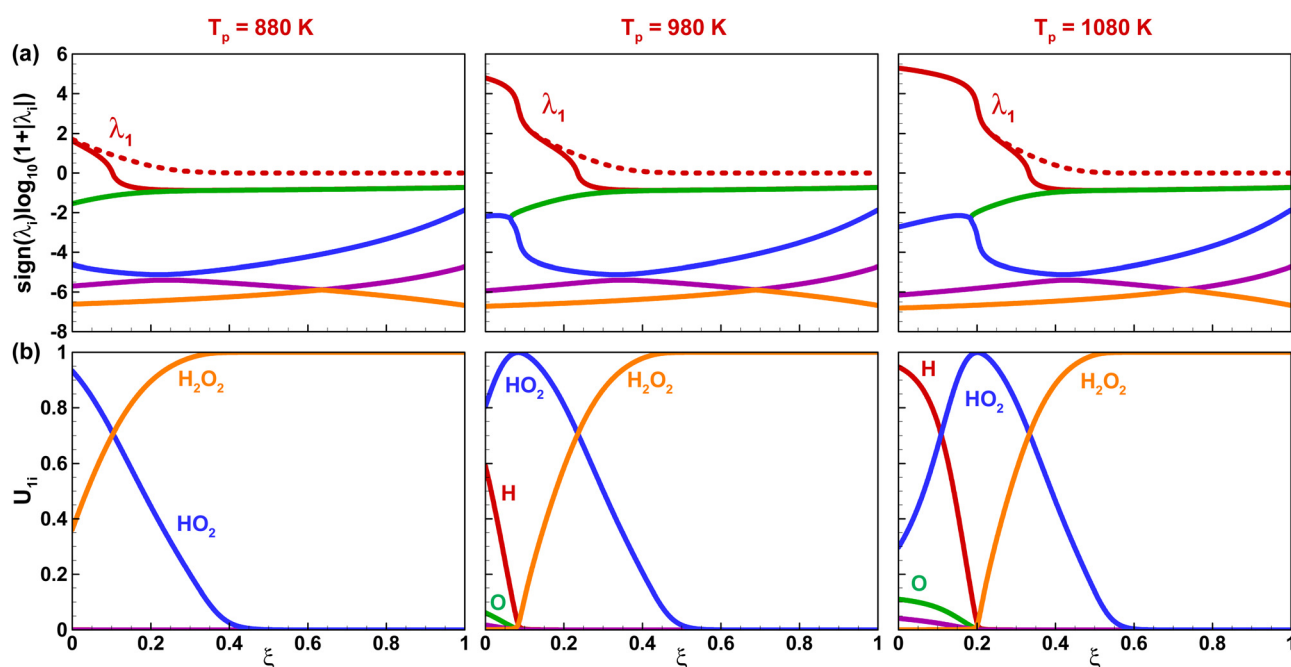


Fig. 1 Variation of (a) the eigenvalue  $\lambda_i$  and (b) components of vector  $U_1$  with  $\xi$  for a stoichiometric  $H_2$ /air mixture (300 K and 1 atm) heated by a hot particle with different temperatures. Dash lines denote the results without the wall destruction effect.

than the ambient  $H_2$ /air mixture, suggesting that the generated chemical radicals are concentrated within a shell with distance  $\delta$  enveloping the particle, whose volume can be estimated as  $4\pi R^2\delta$ . The wall destruction effect can be understood as the radical sticking on the particle surface, depending on the sticking coefficient, the average thermal velocity and the surface-to-volume ratio of the radical containing shell, which accordingly equals to  $1/\delta$ .

In general, the reactions relevant to radical production have high activation temperature, which suggests that the rate of radical generation varies exceedingly rapidly with temperature. It implies that the concentration of the radical tends to be infinitesimal when the temperature falls below a threshold value, according to which the thickness of the radical containing shell can be determined. Specifying this threshold value to be the intermediate temperature between the hot particle and the cool ambient, i.e.,  $T_{\text{threshold}} = (T_p + T_u)/2$ , we obtain the result  $\delta = R$ . Thus, the surface-to-volume ratio is expressed as  $1/R$ , based on which we evaluate the rate of radical termination at the particle surface through the following form

$$k_i = \sigma \bar{v}_i \frac{1}{R} \quad (4)$$

where  $\sigma$  is the sticking coefficient,  $\bar{v}_i$  is the average thermal velocity of species  $i$ , and  $R$  is the particle radius. Existing studies demonstrated that the magnitude of  $\sigma$  ranges from  $10^{-5}$  to  $10^{-2}$  and  $\sigma = 10^{-3}$  is adopted in this work.

For a given reactant mixture, specified by eqn (2), the eigenvalues of  $L$ , denoted by  $\lambda_i$ ,  $i = 1, \dots, 5$ , depends upon the temperature and pressure. The eigenvalues can be obtained through similarity transformation, i.e.,  $A = ULU^{-1}$ , where  $A$  is a diagonal matrix consisting of eigenvalues, and  $U$  is constituted by the corresponding column eigenvectors of  $L$ .

Applying left multiplication of  $(WU)^{-1}$  on both sides of eqn (3) and denoting  $Y_U = (WU)^{-1}Y$ , the individual ODE is decoupled and the second order derivative  $d^2Y/d\xi^2$  splits into three terms, i.e.,  $d^2Y_U/d\xi^2$ ,  $2U^{-1} \cdot dU/d\xi \cdot (dY_U/d\xi)$ ,  $U^{-1} \cdot (d^2U/d\xi^2) \cdot Y_U$ . According to results shown in Fig. 1, the magnitude of  $\lambda_1$  is about  $O(10^5)$  corresponding to the critical ignition state. We may evaluate the coefficient of the reaction term by scaling analysis, giving  $(\lambda_1 R^2)/(D_Y(1-\xi)^4) \sim O(10^3)$ . Since both  $U$  and  $\xi$  are of order  $O(1)$ , it suggests that the value of term  $U^{-1}d^2U/d\xi^2$  should not differ significantly from  $O(1)$ , which, therefore, can be neglected in the subsequent discussion. The scale of  $U$  is  $O(1)$  and so is the second derivative with respect to  $\xi$ , which is much smaller than the reaction term coefficient  $A$  ranging from  $10^4$  to  $10^5$  and thus can be ignored. As a result, we have

$$\frac{d^2Y_U}{d\xi^2} + 2U^{-1} \frac{dU}{d\xi} \cdot \frac{dY_U}{d\xi} = -\frac{R^2}{D_Y(1-\xi)^4} \left\{ AY_U + U^{-1} \frac{W}{\rho} I \right\} \quad (5)$$

Eqn (5) indicates that each component of  $Y_U$  depends on the sign and magnitude of the corresponding eigenvalue  $\lambda_i$ .

### 2.3 Eigenvalue analysis and critical ignition conditions

According to Liang and Law,<sup>23</sup> the accumulating behaviour of radicals during ignition is described by the eigenvalue with the positive real part, denoted by  $\lambda_1$ . The remaining eigenvalues with a negative real part represent the relaxation of radical distributions to equilibrium. The rate of radical accumulation is characterized by the magnitude of  $\lambda_1$ , which tends to be smaller when the effect of wall destruction is taken into account. The eigenvalues of  $L$  can be obtained by numerical calculation. Fig. 1(a) shows that the real part of  $\lambda_1$  reaches the maximum value at particle surface ( $\xi = 0$ ), where the local temperature is the highest. Besides, the real part of  $\lambda_1$  reduces as the particle temperature decreases from 1080 K to 880 K. At intermediate values of  $\xi$ , all eigenvalues become negative, indicating that ignition cannot occur at such distances from the particle surface because of no radical accumulation at relatively low temperature. Therefore, ignition first occurs near the particle surface, which is consistent with the existing numerical and experimental studies.<sup>12,14,29</sup>

The eigenvector corresponding to  $\lambda_1$ , denoted by  $U_1$ , characterizes the normalized mole fraction of the individual radical. Fig. 1(b) shows that the dominant radical close to the particle surface varies with local temperature, which is consistent with Li *et al.*<sup>24</sup> As the particle temperature decreases, the primacy of the H-radical is gradually replaced by the less reactive  $HO_2$  radical. The ignitability of the mixtures is lowered in line with the reduction of  $\lambda_1$  as indicated in Fig. 1(a).

To describe the radical runaway process, we only need to consider the ODE characterized by  $\lambda_1$  in eqn (5). The initiation reactions involving reactants can be packed into the boundary condition according to Li *et al.*<sup>24</sup> Therefore, eqn (5) can be reduced to

$$\begin{cases} \frac{d^2y_{U1}}{d\xi^2} + 2 \left( U^{-1} \frac{dU}{d\xi} \cdot \frac{dY_U}{d\xi} \right)_1 = -\frac{R^2 \lambda_1 y_{U1}}{D_Y(1-\xi)^4}, \\ y_U(0) = y_0, y_U(1) = 0, \end{cases} \quad (6)$$

where  $y_0$  characterizes the non-vanishing mass fraction of the radicals which can be attributed to the ever existence of diffusional loss of radicals at the particle surface.

In this equation, we adopt  $D_Y$  defined in terms of the diffusion coefficients of individual species of radicals, denoted by  $D_i$ , and their corresponding molar fraction in the mixture denoted by  $U_{1i}$ , i.e.,

$$D_Y = \left[ \sum_i (D_i U_{1i})^2 \right]^{1/2} \quad (7)$$

For a given composition of the mixture,  $D_Y$  thus determined shall be considered as a constant parameter. In addition, the diffusion coefficients of radicals depend upon temperature and pressure, which implies that  $D_Y$  should be re-evaluated when either the temperature or pressure is changed.

In analogy to the Arrhenius form of the reaction rate, the eigenvalue  $\lambda_1$  can formally be written as  $\lambda_1 = K e^{-T_a/T}$ , where  $K$  is the reaction frequency factor and  $T_a$  the activation temperature.<sup>24</sup>

Substituting the chemically frozen solution of the temperature given by eqn (2), we get

$$\lambda_1 = Ke^{-T_a/T_p}e^{-Ze\xi} \quad (8)$$

where  $Ze = \beta T_a/T_p$  is the system Zel'dovich number. It is noted that  $e^{-Ze\xi}$  represents the change of the reaction rate in space. With the knowledge of  $\lambda_1$  and its derivative  $d\lambda_1/d\xi$ , the unknown parameters,  $K$  and  $T_a$ , can be determined as

$$K = e^{-T_a/T_p}\lambda_1|_{\xi=0} \quad (9)$$

$$T_a = -\frac{T_p^2}{(T_p - T_u)\lambda_1|_{\xi=0}} \frac{d\lambda_1}{d\xi} \bigg|_{\xi=0}. \quad (10)$$

Substituting eqn (8) into eqn (6), the radical accumulation equation is cast into the form that can be solved based on large activation energy asymptotic analysis as in thermal ignition theory. Following Li *et al.*,<sup>24</sup> we define the small parameter  $\varepsilon = 1/Ze$  and introduce the scaled coordinate  $\chi = \xi/\varepsilon$ . With respect to the scaled coordinate  $\chi$ , the first and second order derivatives of  $Y_U$  are of orders  $O(1/\varepsilon^2)$  and  $O(1/\varepsilon)$  respectively. In leading order approximation, the term  $dY_U/d\chi$  could be neglected in comparison with  $d^2Y_U/d\chi^2$ , and accordingly the equation describing the radical accumulation near the particle surface could be written in the following form

$$\frac{d^2y_U}{d\chi^2} = -Da e^{-\chi} y_U, \quad (11)$$

$$y_U(0) = y_0, y'_U(\infty) = 0,$$

where  $Da$  is the Damköhler number, defined as

$$Da = \frac{Ke^{-T_a/T}}{Ze^2 D_Y / R^2}. \quad (12)$$

The Damköhler number represents the ratio between radical accumulation by the chain-branching reaction and the loss due to diffusion. There exists a critical Damköhler number,  $Da_c$ , beyond which the rate of radical generation exceeds the rate of radical loss resulting from both diffusion and wall destruction, and thus ignition becomes possible.

Eqn (11) can be solved analytically, giving

$$y_U(\chi) = y_0 \frac{J_0(2\sqrt{Da}\sqrt{e^{-\chi}})}{J_0(2\sqrt{Da})}, \quad (13)$$

where  $J_0(x)$  is the zeroth-order Bessel function. Radical runaway occurs when  $y_U$  approaches infinity. According to eqn (13), this occurs when the denominator becomes zero. Therefore, the critical Damköhler number is determined by

$$J_0(2\sqrt{Da_c}) = 0. \quad (14)$$

The first root of  $J_0(x)$  can be calculated numerically, yielding  $x_0 \approx 2.405$ , based on which the critical Damköhler number is  $Da_c \approx 1.446$ .

Eqn (12) demonstrates that  $Da$  is a function of particle radius and it also depends on temperature and pressure *via*  $K$ ,  $T_a$  and  $Ze$ . Therefore, the ignition limits for different particle

sizes can be plotted in the  $T$ - $p$  space as contours corresponding to the required

$$Da = Da_c = 1.446. \quad (15)$$

### 3. Results and discussion

#### 3.1 Critical ignition temperature

It is noted that the parameters  $K$  and  $T_a$ , depending on the eigenvalue  $\lambda_1$ , are actually functions of particle temperature and ambient pressure, and so is the Damköhler number. Therefore, the critical Damköhler number determines the minimum temperature of the particle that leads to ignition, denoted by  $T_{ig}$ , as a function of pressure and particle radius. In numerical simulation, the ignition time  $\tau_{ig}$  is defined as the instant when the heat flux at the particle surface becomes zero. Then, the critical ignition temperature  $T_{ig}$  can be extrapolated based on the exponential relationship between  $\tau_{ig}$  and  $T_p$ , *i.e.*,  $\tau_{ig} = c/\ln(T_p/T_{ig})$ , where  $c$  is a constant.<sup>17</sup>

The  $T_{ig}$  for hot particle induced ignition in  $H_2$ /air mixtures at room temperature and atmospheric pressure has been reported in the existing numerical and experimental studies, which provides additional benchmark results to verify the present theoretical model.

Fig. 2 shows the change in  $T_{ig}$  with  $R$  in a wide range from 0.1 to 10 mm. The simulation results agree well with those reported by Häber *et al.*,<sup>14</sup> which substantiates the accuracy of numerical simulation adopted in the present study. The variation behaviour of  $T_{ig}$  with  $R$  predicted by eqn (15) is fully consistent with that obtained from numerical simulation. It verifies the theoretically obtained ignition criterion by analysing the stability of linear ODE in terms of the eigenvalue of the largest magnitude.

It is seen that reducing  $R$  leads to a considerable increase of  $T_{ig}$ . It suggests that particles of relatively small sizes exhibit a

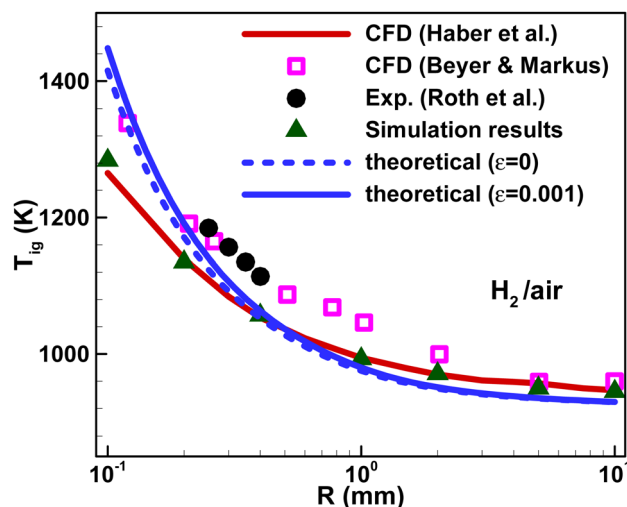


Fig. 2 Variation of the critical ignition temperature with particle radius for a stoichiometric  $H_2$ /air mixture at  $T_u = 300$  K and  $P = 1$  atm. The present theoretical predictions are compared with the experimental data reported by Roth *et al.*<sup>12</sup> and the simulation results from Beyer and Markus,<sup>29</sup> Häber *et al.*<sup>14</sup>



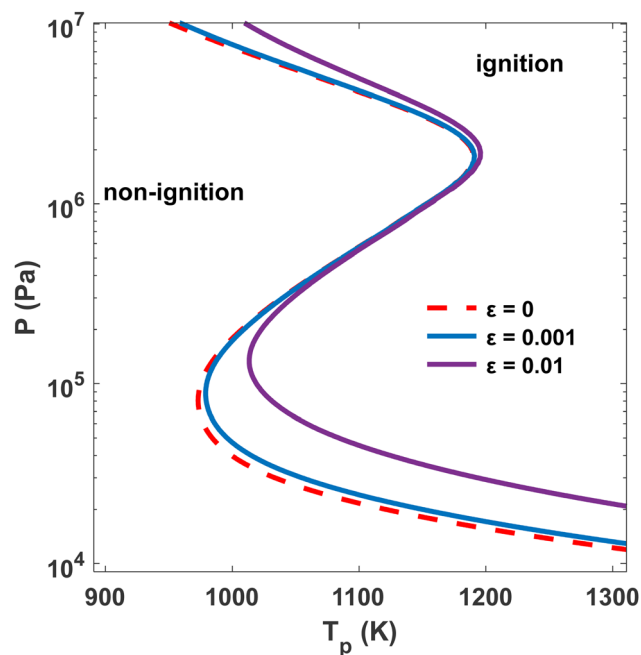


Fig. 3 Change of particle ignition limit with wall destruction effect with different sticking coefficients.

comparably low risk of causing accidental ignition in  $\text{H}_2/\text{air}$  mixtures. This is because the conductive and diffusive loss of heat and radicals on the particle surface becomes more intensive for smaller particles, which require a higher reaction rate to accumulate active radicals and thus higher particle temperature to achieve ignition.

### 3.2 Effects of wall destruction

The wall destruction enhances the radical loss during the ignition process. As Fig. 3 shows, the critical ignition temperature increases with wall destruction, especially for the first and third ignition limits. For  $\sigma = 10^{-3}$ ,  $T_{\text{ig}}$  increases about 10 K. With a larger  $\sigma$ , the wall destruction effect becomes stronger, which leads to higher  $T_{\text{ig}}$ .

The temperature increase in particle ignition caused by the wall destruction of each radical is consistent with the results in homogeneous ignition.<sup>23</sup> Under low pressure conditions, the ignition is controlled by the chain branching reaction of H and O. The destruction of H and O increases the critical ignition temperature in the first limit, and the effect of H destruction is more significant. The second limit is controlled by competition between R1f and R4f, thus, it's less affected by wall destruction. Under high pressure conditions, the chain branching reactions involving radicals  $\text{HO}_2$  and  $\text{H}_2\text{O}_2$  play essential roles during ignition. With wall destruction, the chain branching pathway through  $\text{HO}_2$  and  $\text{H}_2\text{O}_2$  is suppressed, and the temperature increases in the third limit. The destruction of OH has an inconspicuous effect on the ignition limit.

### 3.3 Effects of the particle radius

Compared with the previous studies based on thermal theory adopting a single-step global reaction,<sup>20</sup> this theoretical model

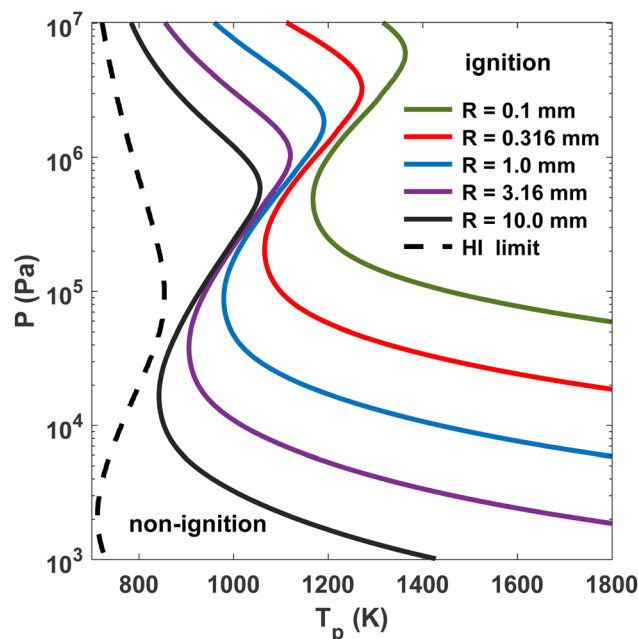


Fig. 4 Variation of the critical ignition temperature with pressure for different radii of the hot particle in a stoichiometric  $\text{H}_2/\text{air}$  mixture at  $T_u = 300$  K. The dashed line refers to the limiting situation of ignition induced by the hot particle with infinitely large radius  $R \rightarrow \infty$ .

quantitatively predicts the ignition limit since the overall effect of essential chain reactions is characterized by  $\lambda_1$ . The presence of a hot particle leads to non-vanishing gradients of temperature and radical concentration at the particle surface. However, such inhomogeneities do not alter the nonmonotonic behaviour of the ignition limit. Fig. 4 shows that ignition limits for different particle radii exhibit Z-shaped curves analogous to the homogeneous  $\text{H}_2/\text{air}$  mixture. A similar behaviour of the ignition limit was also observed for premixed  $\text{H}_2/\text{air}$  ignited by heated nitrogen in the counterflow.<sup>24,30</sup>

Fig. 4 shows that the Z-shaped limit curve shifts to higher temperature and pressure conditions along the line corresponding to the second ignition limit when the particle radius decreases. This is because the net rates of radical accumulation are affected by diffusional loss of radicals around the particle surface which becomes more pronounced for smaller particle radius. The first and third ignition limits depend on the radical concentration. Therefore, the particle size has a strong impact on the position of the first and third ignition limits as shown in Fig. 4. The second limit results from the competition between chain branch reaction R1f and chain termination reaction R4f and can be determined by  $2k_{1f} = k_{4f}[\text{M}]$  which is hardly affected by the radical concentration. Consequently, the second ignition limits for different particle radii collapse on nearly the same curve as shown in Fig. 4.

According to previous experiments,<sup>11,19</sup> there may be a critical size of the particle below which the radicals are unable to sufficiently accumulate and ignition can hardly occur. This phenomenon is also investigated in Wang and Chen's simulation.<sup>17</sup> They found that the ignition delay time increases

with decreasing particle radius. For a sufficiently small radius, the ignition cannot occur because the ignition time approaches infinity. In this work, we consider the ignition taking place in a quiescent environment. The residence time of a gas parcel could be infinitely long since there is no relative motion between the combustible mixture and the hot particle according to the work of Yu and Chen.<sup>21</sup>

The critical ignition condition refers to the state in which the rate of radical loss by diffusion is balanced by the rate of radical production by a chain reaction in the vicinity of the particle surface. Reducing the particle radius leads to stronger radical diffusion away from the particle surface, which implies that a higher rate of radical generation must be associated in the critical ignition state. Thus, a higher particle temperature is required to achieve the ignition. However, the temperature of the particle cannot be infinitely high, and a practical estimation of the upper bound could be about 4000 K. Thus, the critical particle radius for ignition can thus be derived based on this threshold for the particle temperature.

### 3.4 Effects of the Lewis number

For a mixture consisting of multiple species, the diffusion coefficient for individual components varies drastically. The averaged Lewis number of radicals is introduced as  $Le = \alpha/D_Y$ , in which  $D_Y$  represents the molar averaged mass diffusion coefficient for the radicals. According to kinetic theory of gas, the diffusivities pertaining to individual radical species are functions of temperature and pressure. Therefore, the Lewis number should be parametrically calculated when either temperature or pressure changes.

In theoretical studies, it is convenient to adopt the unit Lewis number assumption that forces the mass diffusion

process in a phase with heat conduction. However, for  $H_2$ /air ignition involving H-radical and  $H_2$ , the approximation of unity Lewis number may considerably alter the ignition behaviour. This is demonstrated by the results shown in Fig. 5, in which the deviation between the solid and dashed lines represents the effect of preferential diffusion between heat conduction and mass diffusion during hydrogen ignition induced by a hot particle.

As expected, the second ignition limit hardly changes with  $Le$  because the rate of radical diffusion tends to be insubstantial compared with competing chain branching reaction R1f and chain termination reaction R4f. Moreover, Fig. 5 shows that for each particle size, the solid Z-curve is squeezed compared with the dashed ones. This indicates that the first and third ignition limits are respectively suppressed and facilitated by the effect of preferential diffusion. The cause can be interpreted as follows. At pressures traversing the first ignition limit, the eigenvector  $U_1$  indicates that the dominant radical close to the particle surface is the H radical. The Lewis number of the H radical is much less than unity, suggesting a more severe diffusive loss of the H radical in actual ignition process. Consequently, the first ignition limit moves to the region with higher pressure and temperature when preferential diffusion (*i.e.*, non-unity Lewis number, solid lines in Fig. 5) is considered. At relatively high pressures relevant to the third ignition limit, the eigenvector  $U_1$  indicates that the dominant radical changes to  $HO_2$ , whose Lewis number is greater than unity, implying a slower diffusive loss of the radical at the particle surface. Therefore, the third ignition limit slightly moves to the region with lower pressure

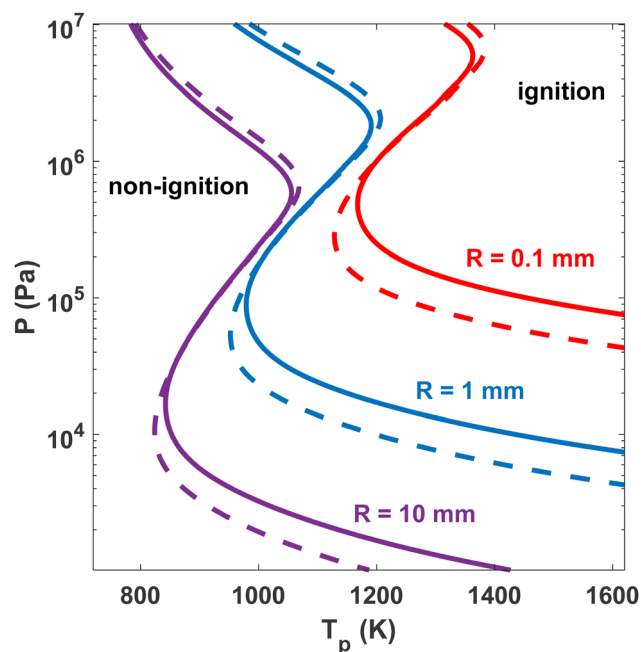


Fig. 5 Variation of the critical ignition temperature with pressure for different radii of the hot particle in a stoichiometric  $H_2$ /air mixture at  $T_u = 300$  K. The dashed/solid lines correspond to ignition limits with/without the assumption of  $Le = 1$ .

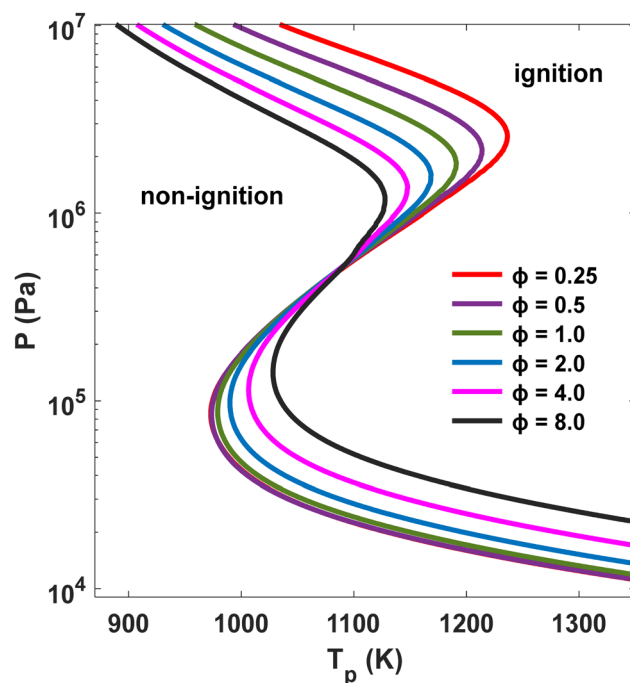


Fig. 6 Variation of the critical ignition temperature with pressure for  $H_2$ /air mixtures with different equivalence ratios at  $T_u = 300$  K. The hot particle radius is  $R = 1$  mm.

and temperature when preferential diffusion (i.e., non-unity Lewis number, solid lines in Fig. 5) is included.

### 3.5 Effects of the equivalence ratio

For most combustible mixtures, the equivalence ratio plays an important role in affecting the ignition behaviour. Fig. 6 shows the ignition limits for  $\text{H}_2/\text{air}$  mixtures at different equivalence ratios subjected to a hot particle of radius 1 mm. The ignition limits remain to be Z-shaped, and the gap between the first and the third ignition limits narrows with increasing equivalence ratio. Whereas the second ignition limit changes slightly with the equivalence ratio. This is because the controlling chain reactions leading to the second limit exhibit weak dependence on the concentration of the reactant.

The dominant reactions for the first ignition limit are R1f, R2f and R3f as listed in Table 1. Increasing the equivalence ratio lowers the concentration of  $\text{O}_2$ , which suppresses the chain branching reaction R1f. Accordingly, it leads to the reduction of the concentrations of O and OH radicals. Subsequently the chain branching and chain carrying reactions are inhibited, which results in the decrease of the total radical generation rate. Accordingly, the first ignition limit moves to the region with higher pressure, producing sufficient concentration of  $\text{O}_2$  to initiate ignition, in association with increasing equivalence ratio.

For the third limit, the dominant reactions are R10f and R12f, the latter of which is enhanced by increasing the hydrogen concentration. As more  $\text{H}_2\text{O}_2$  is generated, the decomposition reaction R10f is facilitated, rapidly generating OH radicals and thus forming a positive feedback. Accordingly, the ignition could proceed under relatively lower pressure conditions, which leads to a uniform decrease of the third ignition limit with increasing equivalence ratio.

The theoretical result in Fig. 7 shows that under atmospheric pressure,  $T_{\text{ig}}$  slightly decreases with  $\phi$  on the extremely

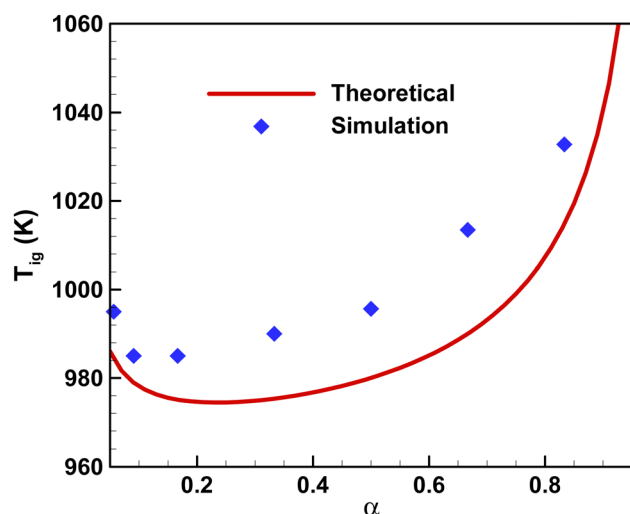


Fig. 7 Variation of the critical ignition temperature with the equivalence ratio of  $\text{H}_2/\text{air}$  mixtures under atmospheric pressure. The hot particle radius is  $R = 1$  mm.  $\alpha$  is defined as  $\phi/(1 + \phi)$ .

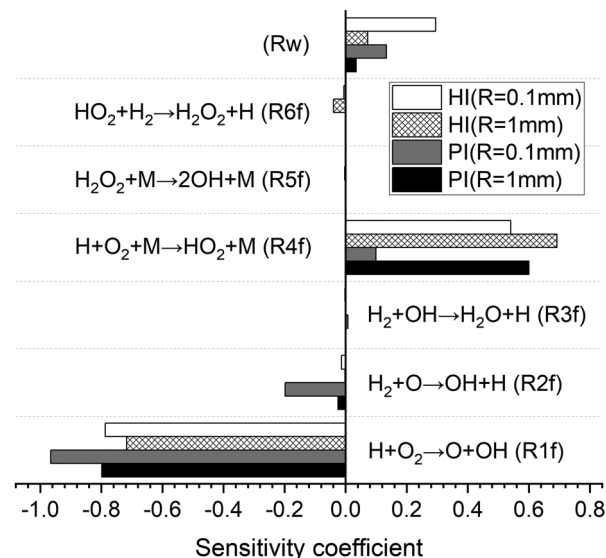


Fig. 8 The components of normalized sensitivity vector corresponding to different radii (1 mm and 0.1 mm) under atmospheric pressure in PI (particle ignition) and HI (homogeneous ignition) systems.

lean side and increases with  $\phi$  on the lean and rich side. The simulation shows a similar result, though the turning point shifts to the lean side. The relative difference between the theoretical and numerical results is within 3%, which demonstrates the validity of theoretical analysis. It is noted that a minimum  $T_{\text{ig}}$  could be sought at the optimum equivalence ratio, denoted by  $\phi_{\text{opt}}$ , the latter of which, however, may be considered as a function of particle radius. In general, varying the equivalence ratio may not lead to a significant change in the critical ignition temperature.

### 3.6 Sensitivity analysis for particle ignition

The Z-curve of particle ignition shows similarity to that in homogeneous ignition. To acquire insights into their difference, we investigate the sensitivity of critical ignition temperature in both the homogeneous ignition (HI) system and the particle ignition (PI) problem to essential chain reactions. Two representative radii, i.e.,  $R = 0.1$  mm and  $R = 1.0$  mm are selected for the PI system, and correspondingly, the HI system of the same dimensions is considered for comparison. The chain reactions are characterized by their individual rate coefficients  $k$ , and thus the sensitivity is calculated as:

$$s_i = \frac{\frac{\Delta T_{\text{ig}}}{T_{\text{ig}}}}{\frac{\Delta k_i}{k_i}} = \frac{\Delta \ln(T_{\text{ig}})}{\Delta \ln(k)} \quad (16)$$

where  $\Delta T_{\text{ig}}$  represents the change of critical ignition temperature due to the variation of the reaction rate coefficient of the  $i$ th reaction  $\Delta k_i$ . Each quantity  $s_i$  refers to a component in the sensitivity vector, defined by  $\mathbf{s} = [s_1, \dots, s_m]^T$ , where  $m$  is the number of reaction paths participating in sensitivity analysis. The sensitivity vector is further normalized, yielding  $\|\mathbf{s}\| = 1$ .



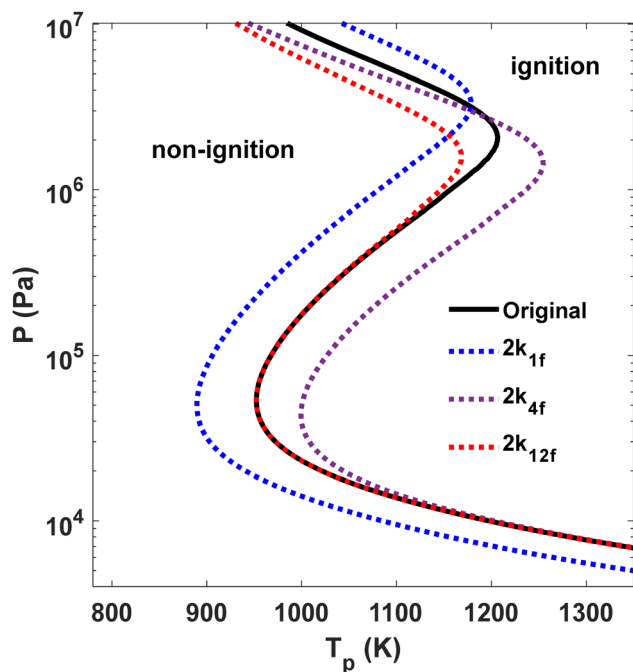


Fig. 9 Variation of the critical ignition temperature with pressure by increasing the rates of key reactions in a stoichiometric  $\text{H}_2/\text{air}$  mixture at  $T_u = 300$  K. The hot particle radius is  $R = 1$  mm.

Fig. 8 shows that the components in  $s$  relating to R1f and R4f are of opposite signs. It could be understood that the critical ignition temperature decreases as R1f becomes stronger, however, it increases as R4f is facilitated. For smaller particles with stronger radical wall (Rw) destruction, the sensitivity of Rw increases, and the critical ignition temperature become higher (975 K to 1432 K for PI, 922 K to 958 K for HI). With a relatively high temperature, the radical accumulation is fast. The wall destruction plays a less important role in PI than that in HI. Meanwhile, the dominant radical accumulation shifts from  $\text{HO}_2$  to H with increasing temperature which we can find from Fig. 1. Thus, in the PI system, the sensitivity of chain-branching reactions R1f and R2f, respectively corresponding to H consumption and H production increases, while the sensitivity of the chain-termination reaction R4f corresponding to  $\text{HO}_2$  radical decreases.

Based on the sensitivity analysis, we found that the primary reactions which can considerably affect the global response of Z-curve are R1, R4 and R12. Fig. 9 compares the Z-curves which are obtained by altering the kinetics of those elementary reactions individually. It was observed that the non-ignition regime relating to the first and second ignition limit regresses almost uniformly to lower temperature when R1f was enhanced, while the third ignition limit shifts to higher temperature. It can be understood that a more rapid chain initiation reaction facilitates the ignition process. The upwards shift of the third limit can be attributed to the competition between R1f and R4f. When R1f is enhanced, it consumes the reactants of R4f and suppresses the chain branching pathway R4f–R12f–R10f. Accordingly, a higher pressure is required to

accelerate the three-body reaction R4f to achieve ignition. As reaction R4f is accelerated to twice magnitude, the first and third ignition limits vary slightly, however, the second ignition limit considerably shifts to the higher temperature regime. This is because R4f can be considered as a chain termination reaction, which diminishes the low-pressure chain branching pathway R1f and inhibits ignition with increasing pressure. Nevertheless, the ignition of the third limit through R4f–R12f–R10f is slightly enhanced due to sufficient  $\text{HO}_2$ . On increasing the rate of R12f, the first and second ignition limits remain because of the relatively low reactivity of  $\text{HO}_2$  under low pressure conditions, while the third limit tends to move downwards, which demonstrates that the reaction pathway R4f–R12f–R10f is accelerated and thus facilitates ignition.

## 4. Conclusions

The ignition of premixed hydrogen/air mixtures by a spherical hot particle is investigated theoretically and numerically. The radical runaway process with the detailed reaction mechanism is investigated through eigenvalue analysis, based on which the radical accumulation equations are reduced into a rate-controlling ODE. The critical ignition Damköhler number is thus determined in terms of the analytical solution of the rate-controlling ODE. The critical ignition particle temperature can be determined as a function of ambient pressure and particle radius. Under atmospheric pressure, the critical ignition temperature of the hot particle predicted by the current theory agrees well with experimental and numerical results over a wide range of particle radii. As the particle size decreases, the Z-shaped ignition curve shifts to a higher temperature and pressure regime along the boundary of the second ignition limit. It is interpreted that the diffusive loss of radicals increases with reducing particle sizes. The preferential diffusion (*i.e.*, non-unity Lewis number) and the increase of the equivalence ratio are found to squeeze the Z-curve, *i.e.*, ignition is suppressed/enhanced at the first/third ignition limit. This can be explained by their influence on the rate of dominant reactions involved in different ignition limits. Compared with homogeneous ignition problems, sensitivity analysis indicates that the relative impacts of essential chain reactions alter due to the presence of inhomogeneity induced by the particle surface. It is noted that the current study assumes no relative motion between the hot particle and the flammable mixture. The impact of ambient flows on the ignition process shall be discussed in our future work.

## Conflicts of interest

There are no conflicts of interests to declare.

## Acknowledgements

This work was supported by the National Natural Science Foundation of China (No. 52176096 and 52006001) and the

Opening Fund of State Key Laboratory of Fire Science (SKLFS) under Grant No. HZ2021-KF01.

## References

- 1 V. Babrauskas, *Ignition Handbook*, Fire Science Publishers, Issaquah, 2003.
- 2 S. A. Coronel, *Thermal ignition using moving hot particles*, California Institute of Technology, Pasadena, California, 2016.
- 3 S. Wang, X. Huang, H. Chen and N. Liu, Interaction between flaming and smouldering in hot-particle ignition of forest fuels and effects of moisture and wind, *International Journal of Wildland Fire*, 2016, **26**, 71–81.
- 4 S. E. Hosseini and B. Butler, An overview of development and challenges in hydrogen powered vehicles, *Int. J. Green Energy*, 2020, **17**, 13–37.
- 5 Z. Abidin, A. Zafaranloo, A. Rafiee, W. Mérida, W. Lipiński and K. R. Khalilpour, Hydrogen as an energy vector, *Renewable Sustainable Energy Rev.*, 2020, **120**, 109620.
- 6 E. Abohamzeh, F. Salehi, M. Sheikholeslami, R. Abbassi and F. Khan, Review of hydrogen safety during storage, transmission, and applications processes, *J. Loss Prev. Process Ind.*, 2021, **72**, 104569.
- 7 B. Lewis and G. Elbe, *Combustion, flames, and explosions of gases*, Academic Press, Orlando, 3rd edn, 1987.
- 8 A. L. Sánchez and F. A. Williams, Recent advances in understanding of flammability characteristics of hydrogen, *Prog. Energy Combust. Sci.*, 2014, **41**, 1–55.
- 9 W. Han, P. Dai, X. Gou and Z. Chen, A review of laminar flame speeds of hydrogen and syngas measured from propagating spherical flames, *Appl. Energy Combust. Sci.*, 2020, **1-4**, 100008.
- 10 R. S. Silver, LXV, The ignition of gaseous mixtures by hot particles, *The London, Edinburgh Dublin Philos. Mag. J. Sci.*, 1937, **23**, 633–657.
- 11 D. Roth, P. Sharma, T. Häber, R. Schiessl, H. Bockhorn and U. Maas, Ignition by mechanical sparks: Ignition of hydrogen/air mixtures by submillimeter-sized hot particles, *Combust. Sci. Technol.*, 2014, **186**, 1606–1617.
- 12 D. Roth, T. Häber and H. Bockhorn, Experimental and numerical study on the ignition of fuel/air mixtures at laser heated silicon nitride particles, *Proc. Combust. Inst.*, 2017, **36**, 1475–1484.
- 13 S. A. Coronel, J. Melguizo-Gavilanes, R. Mével and J. E. Shepherd, Experimental and numerical study on moving hot particle ignition, *Combust. Flame*, 2018, **192**, 495–506.
- 14 T. Häber, T. Zirwes, D. Roth, F. Zhang, H. Bockhorn and U. Maas, Numerical simulation of the ignition of fuel/air gas mixtures around small hot particles, *Z. Phys. Chem.*, 2017, **231**, 1625–1654.
- 15 T. Zirwes, F. Zhang, T. Häber and H. Bockhorn, Ignition of combustible mixtures by hot particles at varying relative speeds, *Combust. Sci. Technol.*, 2018, **191**, 178–195.
- 16 Y. Wang, H. Zhang, T. Zirwes, F. Zhang, H. Bockhorn and Z. Chen, Ignition of dimethyl ether/air mixtures by hot particles: Impact of low temperature chemical reactions, *Proc. Combust. Inst.*, 2021, **38**, 2459–2466.
- 17 Y. Wang and Z. Chen, Effects of particle size on the ignition of Static CH<sub>4</sub>/air and H<sub>2</sub>/air mixtures by hot particles, *Combust. Sci. Technol.*, 2020, **194**, 869–881.
- 18 J. Melguizo-Gavilanes, R. Mével, S. Coronel and J. E. Shepherd, Effects of differential diffusion on ignition of stoichiometric hydrogen-air by moving hot spheres, *Proc. Combust. Inst.*, 2017, **36**, 1155–1163.
- 19 S. Jones, J. Melguizo-Gavilanes and J. E. Shepherd, Ignition by moving hot spheres in H<sub>2</sub>-O<sub>2</sub>-N<sub>2</sub> environments, *Proc. Combust. Inst.*, 2018, **37**, 1597–1604.
- 20 C. K. Law, Ignition of a combustible mixture by a hot particle, *AIAA J.*, 1978, **16**, 628–630.
- 21 D. Yu and Z. Chen, Theoretical analysis on the ignition of a combustible mixture by a hot particle, *J. Fluid Mech.*, 2022, **936**, A22.
- 22 X. Wang and C. K. Law, An analysis of the explosion limits of hydrogen-oxygen mixtures, *J. Chem. Phys.*, 2013, **138**, 134305.
- 23 W. Liang and C. K. Law, An analysis of the explosion limits of hydrogen/oxygen mixtures with nonlinear chain reactions, *Phys. Chem. Chem. Phys.*, 2018, **20**, 742–751.
- 24 S. Li, W. Liang, Q. Yao and C. K. Law, An analysis of the ignition limits of premixed hydrogen/oxygen by heated nitrogen in counterflow, *Combust. Flame*, 2018, **198**, 230–239.
- 25 Z. Chen, Effects of radiation and compression on propagating spherical flames of methane/air mixtures near the lean flammability limit, *Combust. Flame*, 2010, **157**, 2267–2276.
- 26 Z. Chen, M. P. Burke and Y. Ju, Effects of Lewis number and ignition energy on the determination of laminar flame speed using propagating spherical flames, *Proc. Combust. Inst.*, 2009, **32**, 1253–1260.
- 27 P. Dai and Z. Chen, Supersonic reaction front propagation initiated by a hot spot in *n*-heptane/air mixture with multi-stage ignition, *Combust. Flame*, 2015, **162**, 4183–4193.
- 28 J. Li, Z. Zhao, A. Kazakov and F. L. Dryer, An updated comprehensive kinetic model of hydrogen combustion, *Int. J. Chem. Kinet.*, 2004, **36**, 566–575.
- 29 M. Beyer and D. Markus, Ignition of explosive atmospheres by small hot particles: Comparison of experiments and simulations, *Sci. Technol. Energ. Mater.*, 2011, **73**, 1–7.
- 30 T. G. Kreutz and C. K. Law, Ignition in nonpremixed counterflowing hydrogen versus heated air: Computational study with skeletal and reduced chemistry, *Combust. Flame*, 1998, **104**, 157–175.